Chapter 18
LEAP-UCD-2017 Centrifuge Tests at NCU

Wen-Yi Hung and Ting-Wei Liao

Abstract Liquefaction Experiments and Analysis Projects (LEAP) aim to use simple centrifuge modeling tests to validate and calibrate the numerical modeling results. In LEAP-UCD-2017 project, the design and specification of the model are quite uncomplicated than that of the earlier stage of LEAP. The model stored in a rigid container was construted by medium dense sand with 5 degrees of slope and subjected to a 1-Hz sinusoidal wave of base motion. Models were built, tested and cross-validated by many different research institutes. This paper describes in detail the result of experiments carried at National Central University (NCU), Taiwan (R.O.C.) This paper describes in details the unique part of the experiments at NCU.

18.1 Introduction

Since the 1960s, soil liquefaction is an important issue all over the world. In order to gain further insight into this issue, physical modeling and numerical modeling are widely used to simulate and investigate the behaviors of soil liquefaction. In fact, numerical simulations cannot prove its preciseness and applicability without good parameter correction and verification from the results of physical modeling. Therefore, many projects have been proposed to evaluate the effectively between numerical simulations and physical modeling tests, and early period works such as VELACS project (Arulanandan and Scott 1993–1994) tried to verify the accuracy of various analytical procedures, but the results were not conclusive at the end. In recent years, the experimental techniques used in centrifuge modeling and the instrumentation employed have improved significantly. Hence, a new international cooperation project called Liquefaction Experiments and Analysis Projects (LEAP) is carried out (Manzari et al. 2015). Several centrifuge facilities from the USA, UK, China, Japan, Korea, and Taiwan are participating in the LEAP.

W.-Y. Hung (✉) · T.-W. Liao
Department of Civil Engineering, National Central University, Taoyuan, Taiwan
e-mail: wyhung@ncu.edu.tw

© The Author(s) 2020

B. Kutter et al. (eds.), *Model Tests and Numerical Simulations of Liquefaction and Lateral Spreading*, https://doi.org/10.1007/978-3-030-22818-7_18

For the LEAP-UCD-2017, NCU conducted three centrifuge modeling tests by the geotechnical centrifuge at the NCU centrifuge laboratory. The one-dimensional shaking table on the centrifuge at NCU is capable of offering different kinds of input motions used in the LEAP exercise.

18.2 Test Equipment and Materials

18.2.1 Shaking Table on Geotechnical Centrifuge and Rigid Container

The geotechnical centrifuge in NCU has nominal radius of 3 m and a one-dimensional servo-hydraulic-controlled shaker which is assembled on its swing basket, as shown in Fig. 18.1a. The shaker has a capacity to hold a maximum mass of 400 kg at a maximum acceleration field of 80 g corresponding to maximum nominal force of 53.4 kN. The maximum table displacement is ±6.4 mm with a maximum input frequency of 250 Hz. The payload mounting area of the shaker is 1000 mm (length) × 550 mm (wide).

The container used for LEAP is a rigid box composed by aluminum alloy plates as shown in Fig. 18.1b. The inner dimensions are 767 mm (length) × 355 mm (width) × 400 mm (height), and the net weight of empty box is 106.8 kg.

18.2.2 Sand Material

Ottawa sand (denoted as F-65) is provided by UC Davis and used to prepare and construct the gentle slope models in the LEAP. This kind of sand is a uniform clean sand and can be classified as SP (poorly graded sand) in the Unified Soil Classification System (USCS). The distribution curve of particle size of the Ottawa sand is shown in Fig. 18.2. It can be recognized that finer content is insignificant as the passing amount through No. 200 sieve is approximately 0.2% of total sand weight,

Fig. 18.1 (**a**) Geotechnical centrifuge at NCU (**b**) Rigid container

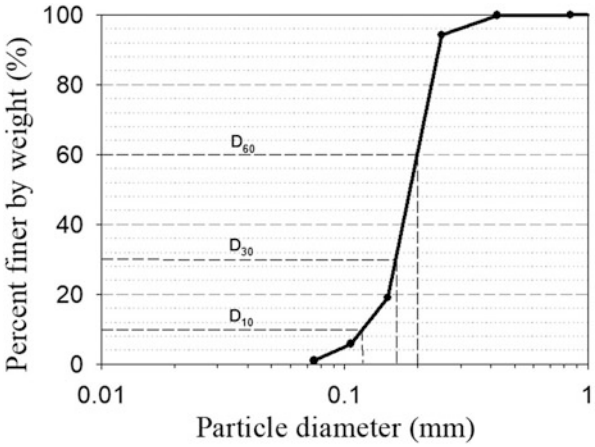

Fig. 18.2 Particle size distribution of Ottawa sand (F-65)

the residual weight passing through No. 100 sieve is around 92.0%, and passing amount through No. 140 sieve is about 6.0% of total weight. Based on those observations, it demonstrated that the sand particle is very small and uniform. Some other physical parameters include specific gravity (G_s) of 2.66 and the mean diameter (D_{50}) of 0.203 mm.

The maximum and minimum dry unit weights under modified ASTM (American Society for Testing and Materials) method are 16.80 and 14.1 kN/m^3 measured by NCU, respectively, but they are 17.24 and 14.62 kN/m^3 measured by UCD (Carey et al. 2019). The target unit weight of slope model in LEAP is 16.20 kN/m^3 which corresponding with 80% of relative density according to NCU max-min dry unit weight result and 64% following UCD's results. Although there is a significant different in relative density, it is no doubt that the centrifuge models in different facilities are similar due to the use of identical material and unit weight.

18.3 Tests Arrangement

18.3.1 Arrangement of the Centrifuge Model

As Fig. 18.3a, b shows that the longitudinal and cross sections of the specific arrangement follow the patterns of the LEAP-2017 project (Kutter et al. 2017), the model is constructed as a 5 degree-inclined saturated sandy slope with 4 m deep in prototype scale (153.8 mm in model type) at the middle of slope and 20 m long in prototype scale (767.0 mm in model type).The target unit weight is 16.20 kN/m^3, which is corresponding to a relative density of 65% as a medium dense sand. The curvature of ground surface relates to effective radius as 2.714 m, which is the distance from ground surface to rotation center of centrifuge, as shown in Fig. 18.3b.

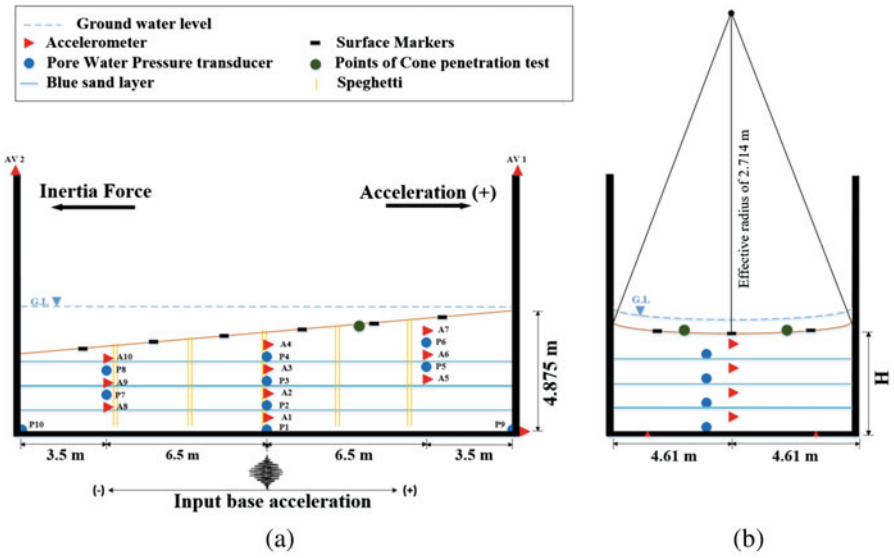

Fig. 18.3 The arrangement of the centrifuge model (**a**) Longitudinal section (**b**) Cross section

There are totally ten accelerometers and eight pore water pressure transducers embedded into the strata divided into three arrays along depth from upslope to downslope, and the interval between each two sensors is constant. Besides, one accelerometer was fixed on the shaker, and two accelerometers are vertically assembled on the top of the rigid container to measure the rocking of container during shaking. Two of pore water pressure transducers were installed at the bottom corner of container. There are a total of 18 polyvinyl chloride (PVC) circular surface makers with outer diameter of 26 mm and inner diameter of 23 mm, and they are put as three arrays at the certain location on the ground surface as indicated in Fig. 18.3a. Three thin blue sand layers are placed at the same elevations of pore pressure transducers P4, P3, and P2 with depth at middle slope of 38 mm, 77 mm, and 115 mm, respectively. Several spaghetti noodles were inserted vertically into the soil deposit.

In this study, the positive acceleration defines that the shaking table moves toward the right side (positive x-axis direction), and the slope dip direction is toward the left side (negative x-axis direction). Thus, the inertial force caused by positive acceleration is toward negative x-axis direction.

18.3.2 Input Base Motions

Three centrifuge modeling tests labeled as NCU 1, NCU 2, and NCU 3 were conducted with different input main-shaking events. Every test has two main-shaking events to investigate the effects of input motion waveforms on inclined saturated slope. Tables 18.1, 18.2, and 18.3 show the fundamental characteristics of

Table 18.1 Fundamental characteristics of input motions for model NCU 1

	Shape of wave	Frequency (Hz)	Number of cycles	Isolated 1 Hz signal	Isolated noise	Achieved base motion	PGA effective
Pre-shaking	SW	3	1	–	–	0.09	–
Motion 1	TSW	1	16	0.18	0.09	0.27	0.22
Post-shaking	SW	3	1	–	–	0.09	–
Post-shaking	NTSW	3	1	–	–	0.09	–
Stop testing temporarily							
Pre-shaking	SW	3	1	–	–	0.09	–
Motion 2	SW	1	16	0.18	0.10	0.27	0.23
Post-shaking	SW	3	1	–	–	0.09	–
Post-shaking	NTSW	3	1	–	–	0.09	–

Table 18.2 Fundamental characteristics of input motions for model NCU 2

	Shape of wave	Frequency (Hz)	Number of cycles	Isolated 1 Hz signal	Isolated noise	Achieved base motion	PGA effective
Pre-shaking	SW	3	1	–	–	0.09	–
Motion 1	TSW	1	16	0.15	0.07	0.22	0.19
Post-shaking	SW	3	1	–	–	0.09	–
Post-shaking	NTSW	3	1	–	–	0.09	–
Stop testing temporarily							
Pre-shaking	SW	3	1	–	–	0.09	–
Motion 2	NTSW	1	16	0.15	0.09	0.25	0.20
Post-shaking	SW	3	1	–	–	0.09	–
Post-shaking	NTSW	3	1	–	–	0.09	–

each motion for three tests. Before every main-shaking, a small 1-cycle sine wave of pre-shaking is applied to detect the shear wave velocity along depth and to identify the initial condition before main-shaking.

There are two main shaking events (Motion-1 and Motion-2) act on each model, all of them have the same frequency of 1 Hz and 16 number of cycles but different in

Table 18.3 Fundamental characteristics of input motions for model NCU 3

	Shape of wave	Frequency (Hz)	Number of cycles	Isolated 1 Hz signal	Isolated noise	Achieved base motion	PGA effective
Pre-shaking	SW	3	1	–	–	0.10	–
Motion 1	TSW	1	16	0.12	0.06	0.18	0.15
Post-shaking	SW	3	1	–	–	0.10	–
Post-shaking	NTSW	3	1	–	–	0.10	–
Stop testing temporarily							
Pre-shaking	SW	3	1	–	–	0.09	–
Motion 2	SW	1	16	0.12	0.07	0.19	0.15
Post-shaking	SW	3	1	–	–	0.10	–
Post-shaking	NTSW	3	1	–	–	0.10	–

SW sine wave, *TSW* tapered sine wave, *NTSW* negative tapered sine wave

amplitude and waveform. Motion 1 is a tapered sine wave that applied in three models and returned three different peak base accelerations (PBA) which are 0.27 g, 0.22 g and 0.18 g, respectively. In NCU-1 and NCU-3 model, Motion 2 is a common sine wave and also yield two values of PBA which are 0.27 g and 0.19 g. Lastly, Motion 2 in NCU-2 is a negavtive tapered sine wave and provide 0.25 g PBA.

After every main-shaking, two small 1-cycle sine waves of post-shakings are applied to detect the shear wave velocity change along depth and to identify the soil properties again after main-shaking. For the two post-shaking, one is sine wave (SW) and another is negative sine wave (NTSW).

18.4 Test Procedure

18.4.1 Model Pluviation

The models were prepared by air pluviation using No. 16 sieve as shown in Fig. 18.4. The flow rate and drop height must be determined to achieve the specific dry unit weight. Therefore, the flow rate of sand mass is controlled at approximately 2.5 kg/minute for passing the opening size of 1.18 mm with three slender slots. The travel path during pluviation is shown in Fig. 18.5. A constant drop height of 0.5 m was used due to the relationship between drop height and dry unit weight under a specific flow rate as shown in Fig. 18.6. The elevation of the sieve above the container during pluviation should be frequently adjusted to maintain a constant

Fig. 18.4 The pluviation equipment

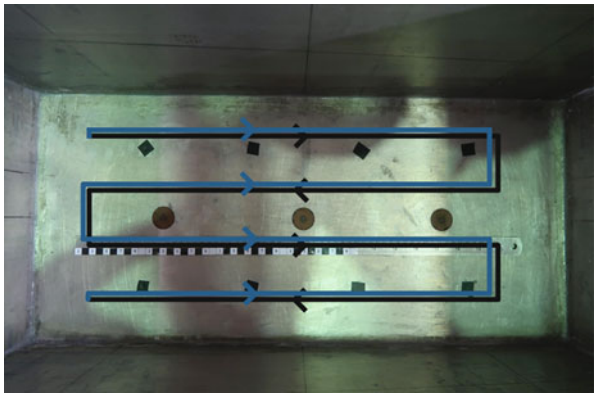

Fig. 18.5 The travel path during deposition

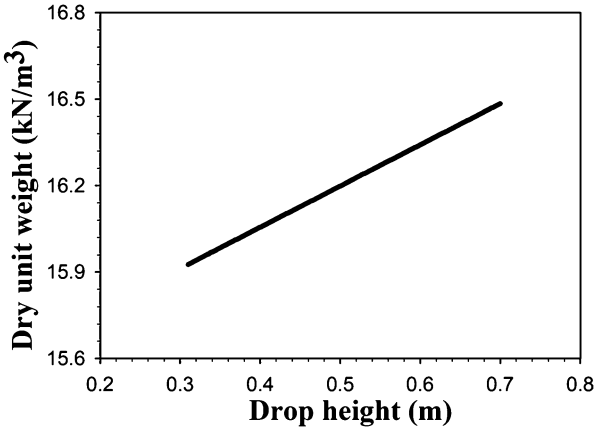

Fig. 18.6 The relationship between dry unit weight and drop height

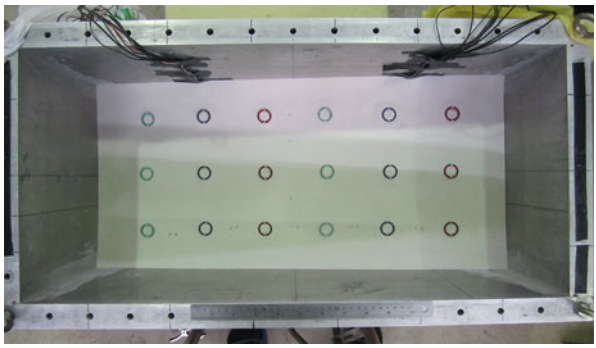

Fig. 18.7 The top view of the dry sample

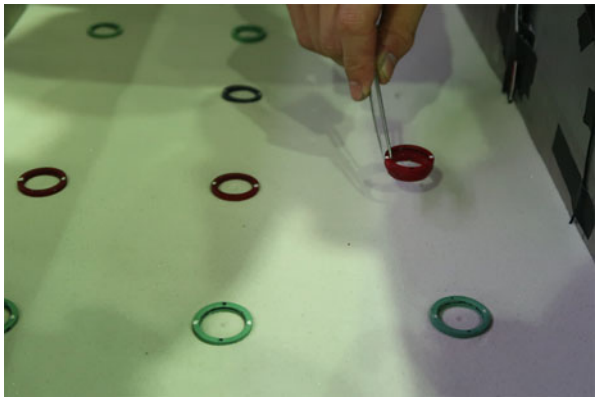

Fig. 18.8 Embedment of surface markers

drop height from the sieve to the sand surface. The ground surface was required to achieve a curved surface, according to the effective radius of the geotechnical centrifuge of 2.714 m.

When pluviated to specific depths, the accelerometers and pore water pressure transducers were embedded at the specific location to measure the time histories of acceleration and pore water pressure during test, and also colored sand was pluviated as a thin color sand layer to observe the circumstances of settlement and lateral spreading. After completing the slope, the surface makers were put on the specific location to record dynamic displacement by cameras during test, and the spaghetti noodles were inserted into strata to observe the circumstances of settlement and lateral spreading. Figure 18.7 shows the top view of the dry model after pluviation was completed. Figures 18.8 and 18.9 show the method used to insert the surface markers and spaghettis, respectively.

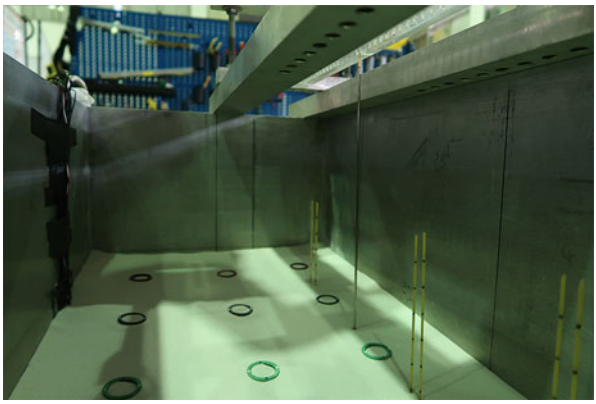

Fig. 18.9 Insertion of noodles

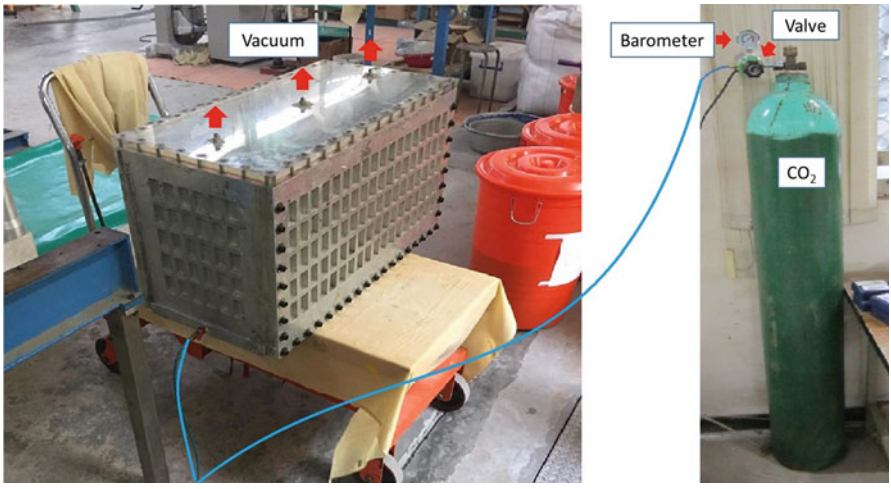

Fig. 18.10 CO_2 system

18.4.2 Model Saturation

Before fluid saturation, a cap was fixed on the top of aluminum container, and the air is vacuumed out from the channels of cap. Then the pure CO_2 floods the model from the bottom of container to fill the voids as shown in Fig. 18.10. The duration is 1.5 h with pressure of 0.25 kg/cm^2 monitored from the barometer. There is not enough space to assemble the frames for laser displacement transducer (LDT) during the following saturation process, and then the aluminum container was placed into a large container and the cap was removed. Frames and LDT are installed on the top of aluminum container. A thin polystyrene plate is placed on the slope surface to measure the water level height by LDT for validating the degree of saturation (Okamura and Inoue 2012). Another bigger acrylic cap and rubber o-ring were

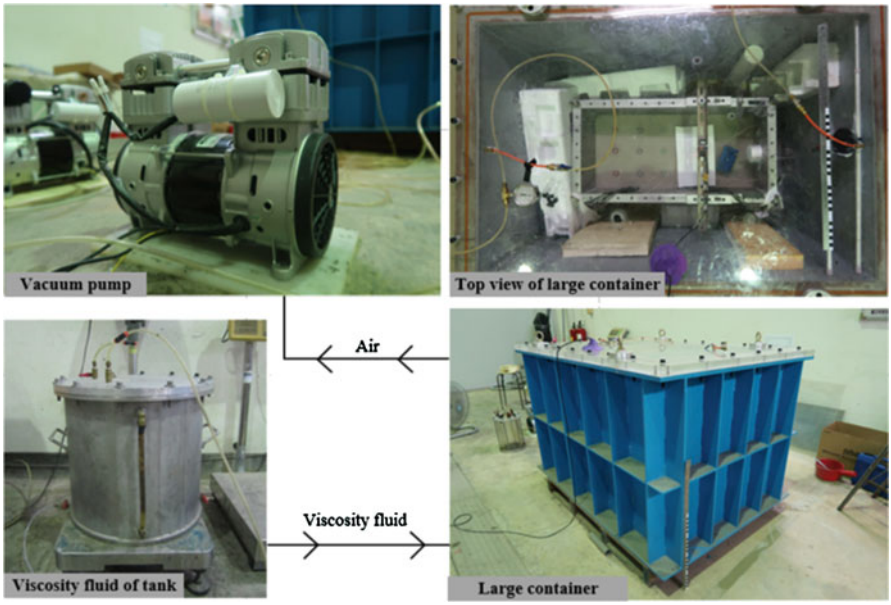

Fig. 18.11 Saturation system

used to seal the large saturation container, and Fig. 18.11 shows the whole saturation system. A vacuum pump is connected to the large container until a stable vacuum pressure of 68 cmHg (91 kPa) is obtained. The methylcellulose liquid with 26 times the viscosity of water is dropped on the slope model to saturate with flow rate of about 2.0 kg/h. A total liquid weight is 27.0 kg after completely soaking the whole model.

Based on Okamura's method, the higher degree of saturation of soil leads to the smaller change in water level at different vacuum pressure according to Eq. 18.1:

$$\Delta h = (1 - S_r)\frac{e}{e+1}\frac{V}{A}\left(\frac{p_1}{p_2} - 1\right) \tag{18.1}$$

where p_1 and p_2 are the chamber pressure (from p_1 to p_2), Δh is the change of water level, S_r is the degree of saturation, e is the void ratio, V is the volume of model, and A is the horizontal section area of model. In Okamura and Inoue's study, the vacuum pressure varies from 15 kPa to 0 kPa(atmospheric pressure). In this study, the degree of saturation is 99.83% if the chamber vacuum pressure changes from 27 kPa to 0 kPa. But it reduces to about 99.4% when the chamber releases higher vacuum pressure. Since the saturation increases with pressure, the degree of saturation of the centrifuge model under positive pore pressure is expected to be greater than 99.8%.

18.4.3 Centrifuge Modeling Procedure

The completed model is then put on the platform of NCU geotechnical centrifuge. Figures 18.12 and 18.13 show the arrangement of model including cone penetration test (CPT) and camera systems. There are five cameras assembled at the top acrylic cap of container, and two sets of CPT cones with two cylinders were installed on the platform. The centrifuge modeling test is shown in Fig. 18.14. Firstly, the model is spun up to 26 g to simulate the same prototype as specified by Kutter et al. (2019—specifications paper, this proceedings). During testing, a non-destructive detect technique, defined as pre-shaking, is triggered before and after main-shaking to measure the shear wave velocity and to estimate the natural frequency of soil strata. It is a 3 Hz, 1 cycle, around 0.066 g (prototype) peak base acceleration sine pulse. Also, before and after the main-shaking, the cone penetration test (CPT) is done by two sets of CPT systems. The resistance is measured by load cell, and displacement

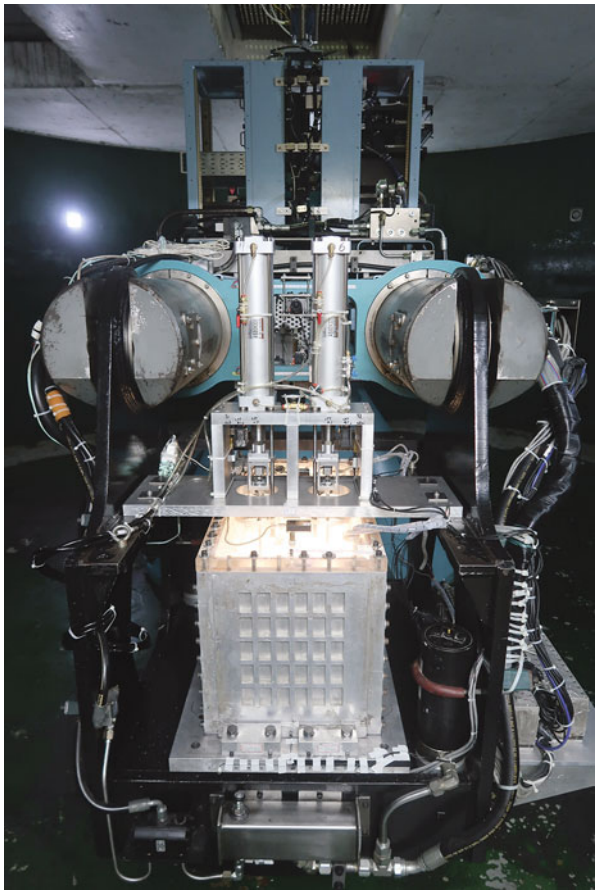

Fig. 18.12 The arrangement of centrifuge modeling test

Fig. 18.13 Equipment of cone penetration test

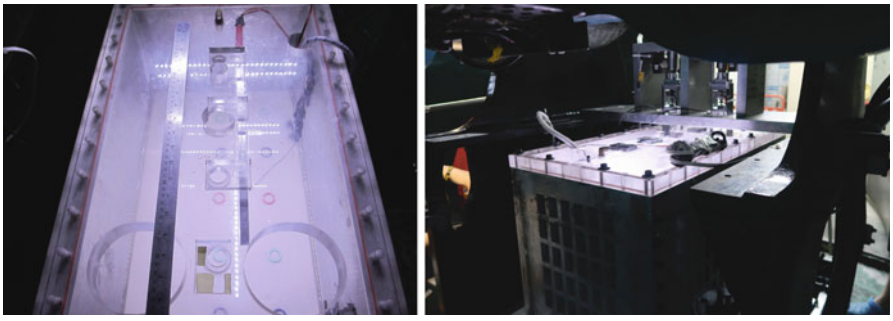

Fig. 18.14 The arrangement of cameras installed at the top of the container

is measured by laser displacement transducer. After finishing the first main-shaking test, the centrifuge is stopped to measure the elevation and the x and y positions on the ground surface, and one set of main-shaking test is completed. The second set of main-shaking centrifuge modeling is then continued with for the same model. Finally, the tested model is cut to detect the deformation of blue thin sand layers and spaghettis. Figure 18.15 shows the process of LEAP tests in NCU.

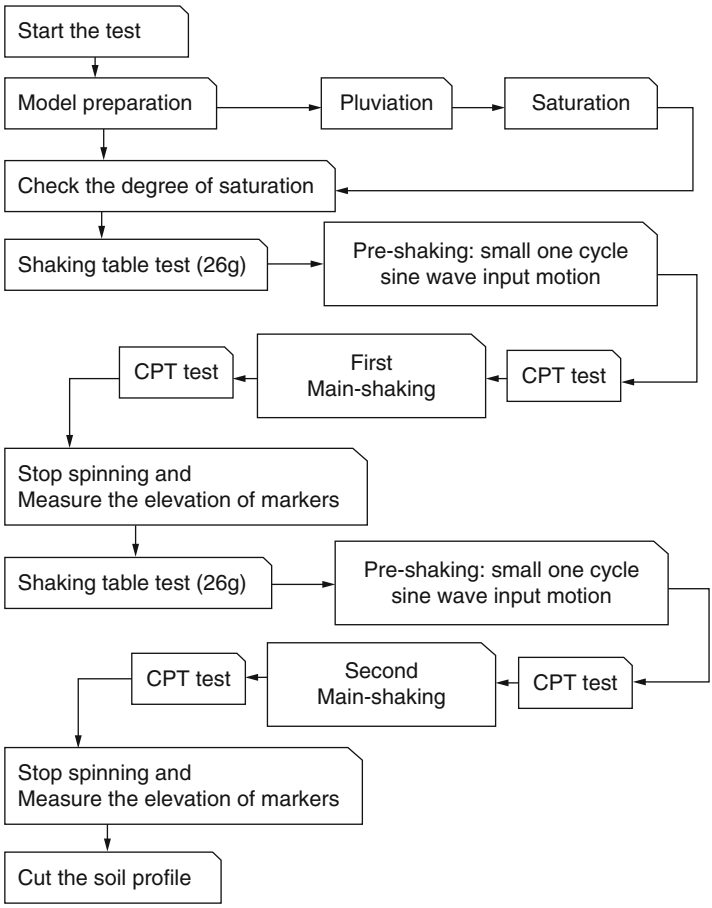

Fig. 18.15 The process of LEAP tests in National Central University

18.5 Results

18.5.1 Acceleration Response and Pore Pressure Response

Figure 18.16 illustrates the acceleration time histories of models NCU 1-M1 (PBA 0.27 g), NCU 2-M1 (PBA 0.22 g), and NCU 3-M1 (PBA 0.18 g) by red, blue, and black lines, respectively. Figure 18.17 shows the acceleration time histories of models NCU 1-M1 (PBA 0.27 g), NCU 2-M1 (PBA 0.22 g), and NCU 3-M1 (PBA 0.18 g) at middle slope array. On the basis of these two figures, all of them have the same phenomenon, and the shape of wave becomes incomplete as the depth under the ground surface decreases. The average of peak amplitude in each cycle of acceleration during the shaking section would attenuate due to the soil strata

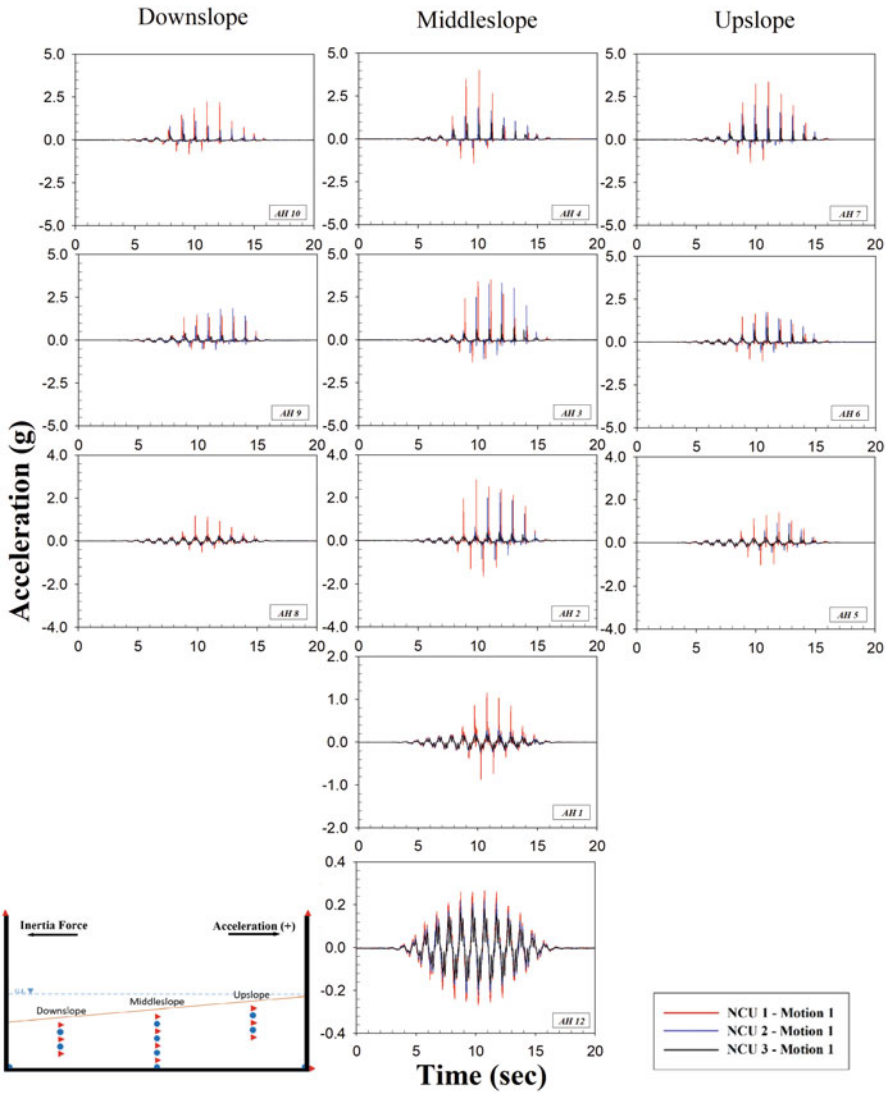

Fig. 18.16 Time histories of acceleration for models NCU 1-M1, NCU 2-M1, and NCU 3-M1

softening. In NCU 1-M1 at the depth of 3.5 m, the strata softened until to the shallowest of the accelerometers. The similarity can be observed at model NCU 2-M1 and NCU 3-M1 at the depths of 3.5 m and 2.5 m, respectively.

When soil strata cannot propagate the shear wave during liquefaction, it is explained due to the effective stress approaching zero; simultaneously, the acceleration amplitude would attenuate and even approach to zero without the spikes. In NCU 1-M1 at the depth of 3.5 m, the shape of wave is observed sufficiently, and the

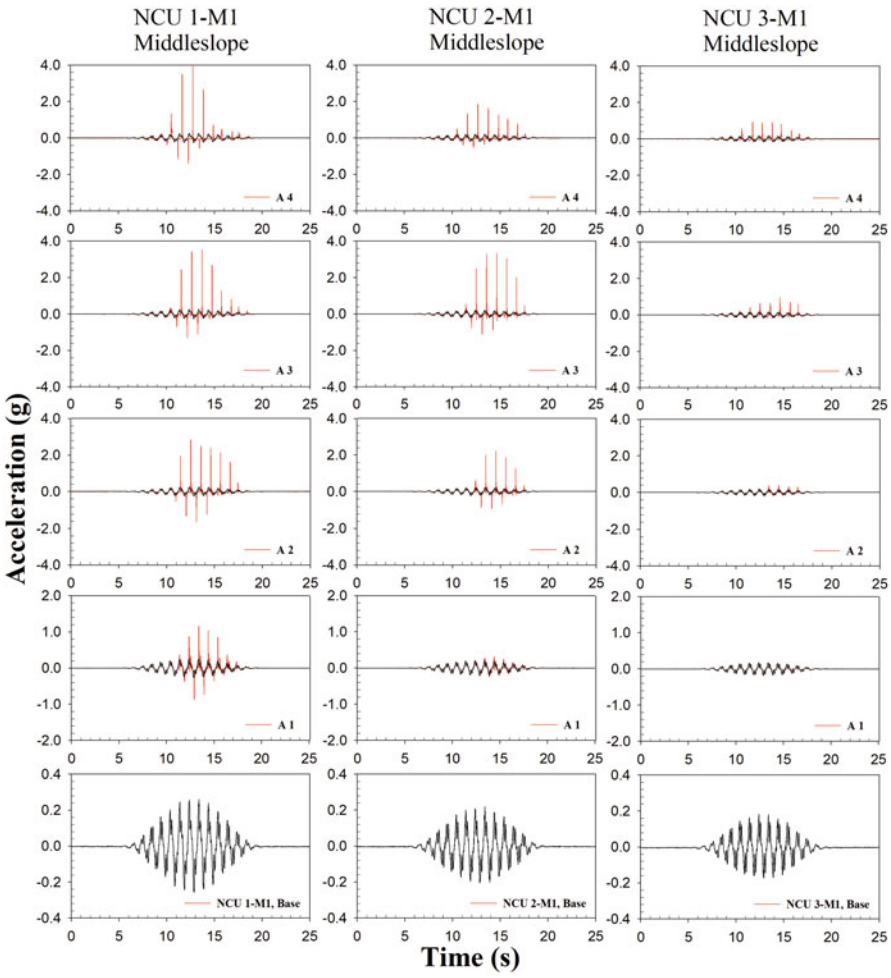

Fig. 18.17 Time histories of acceleration for models NCU 1-M1, NCU 2-M1, and NCU 3-M1 at middle slope

attenuation of acceleration is observed at the 11th cycle, 10th cycle, and 9th cycle on depths of 2.5 m, 1.5 m, and 0.5 m, respectively, which means the soil liquefied at that time. In NCU 2-M1 at the depth of 3.5 m, a complete shape of wave is observed, and the attenuation of acceleration is catched at the 11th cycle, 9th cycle, and 7th cycle at depths of 2.5 m, 1.5 m, and 0.5 m respectively. In NCU 3-M1 at the depth of 1.5 m, the shape of wave is still complete, and the attenuation of acceleration is observed at the ninth cycle at the depth of 0.5 m. In summary, different amplitude of PBA would affect the required duration to reach liquefaction as also the depth of liquefaction.

Figure 18.18 illustrates the pore water pressure ratio time histories of models NCU 1-M1 (PBA 0.27 g), NCU 2-M1 (PBA 0.22 g) and NCU 3-M1 (PBA 0.18 g) by red, blue and black lines, respectively. The excess pore water pressure ratio

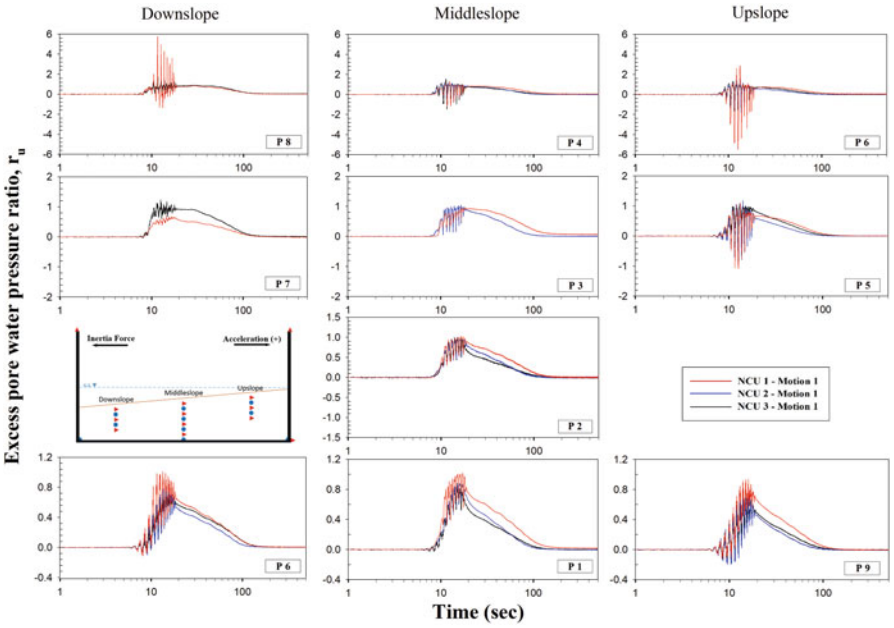

Fig. 18.18 Time histories of pore water pressure for models NCU 1-M1, NCU 2-M1, and NCU 3-M1

achieved 1 at 1 meter depth in each test means that the soil strata is completely liquefied. Liquefaction happened at 2 m depth only in case NCU 1-M1. The pore water pressure in case NCU 1-M1 took the longest time to complete its dissipation than in cases NCU 2-M1 and NCU 3-M1. The waveforms of P9, P1, and P10 installed at the bottom of container are very similar to shaking histories.

In this paper, the coordinate system is indicated in Fig. 18.3. The positive acceleration means the shaking table moves toward upslope (positive *x*-axis direction), and the slope dip direction is toward downslope (negative *x*-axis direction). It is a different sign convention than other facilities. For the following figures, the response of upslope is also put at the right side and that of downslope is at the left side. As shown in Fig. 18.19, there are prominent amplitudes of spikes appearing in the phase where the positive accelerations exist at any depths of the upper slope array and the center slope array, especially in the cases NCU 1-M1 and NCU 2-M1, which is applied for large base acceleration. Because the direction of slope dip is toward the direction of negative base acceleration, it is opposite to the direction of the first half cycle of base acceleration. To demonstrate prominent amplitudes of spikes which appear in the phase of the positive acceleration, the shear strain induced by inertial force from the first half of time history of base acceleration coincides with the direction of slope dip, soil strata would dilate by the shear strain that conducted excess pore water pressure exciting by shaking decrees immediately, and effective stress of soil also increases at once too, so that it can propagate shear wave simultaneously. By contrast, the prominent amplitudes of spikes occur in the

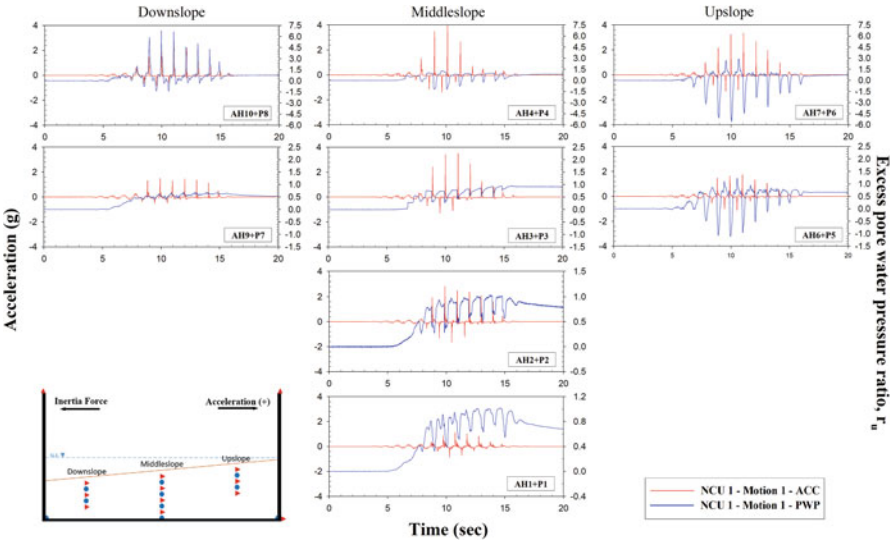

Fig. 18.19 The acceleration and excess pore water pressure histories of model NCU-1

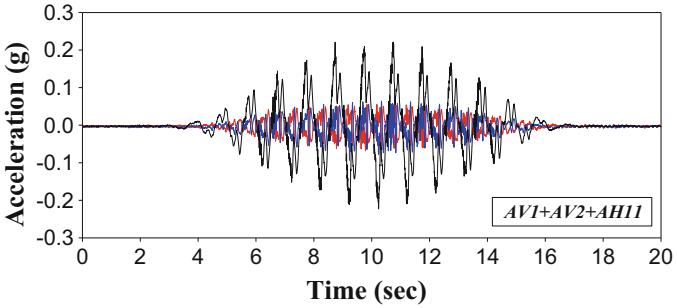

Fig. 18.20 Time histories of acceleration for AV1 and AV2 and AH11 in NCU 2-M1

phase of the positive acceleration histories at the lower slope; however, these spikes accompany with peak value of pore water pressure at the same time. The excess pore water pressure is higher several times than effective stress, especially the pore water pressure transducers are located at the lower part of the slope. This issue is discussed later in this chapter.

Figure 18.20 demonstrates the acceleration time histories of AV1, AV2, and AH11, by red, blue, and black lines in case NCU 2-M1, correspondingly. AV1 and AV2 have the same value of peak ground motion of about 0.05 g. The waveform of AH11 and AV2 is presented at the same phase of wave; however, the phase of waveform of AV1 is opposite to AH11, suggesting that the vertical accelerations are caused by rocking of the container.

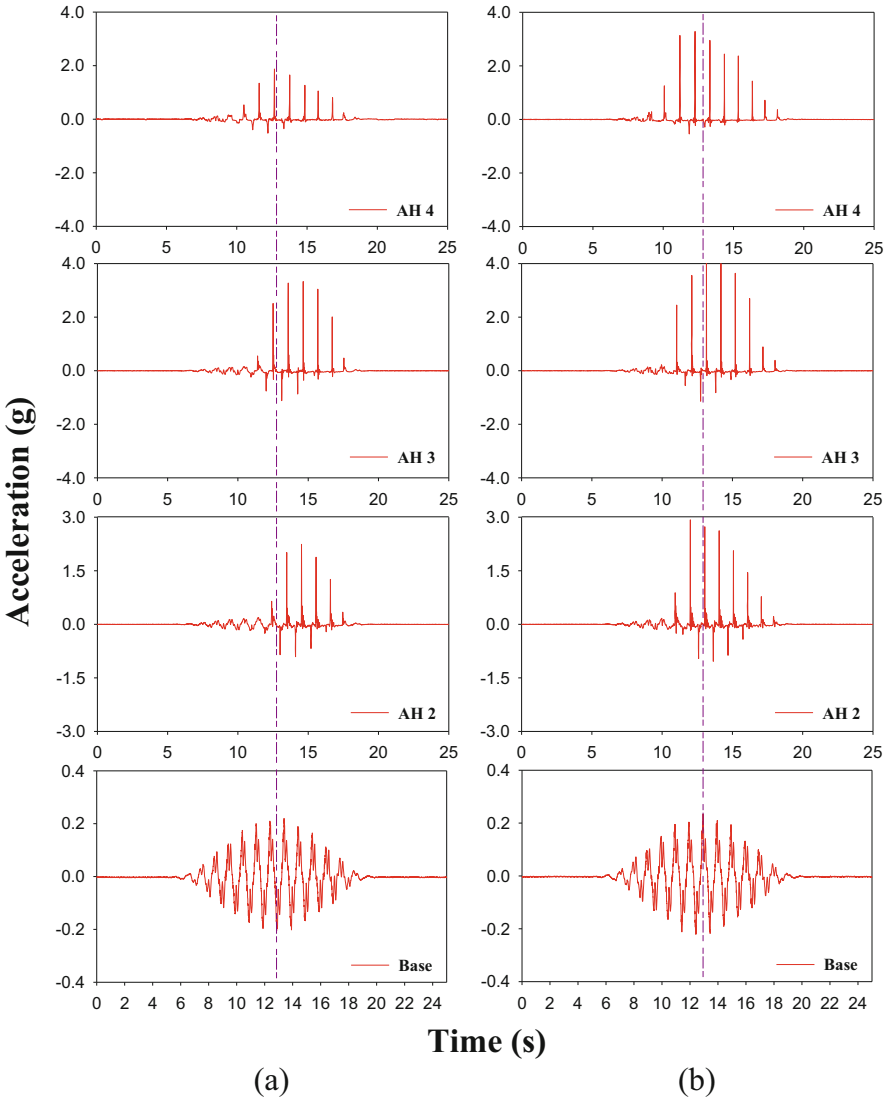

Fig. 18.21 Time histories of acceleration at the middle slope. (**a**) NCU 2-M1 (**b**) NCU 2-M2

Figure 18.21 indicates the acceleration time histories at the middle slope in cases NCU 2-M1 and NCU 2-M2. The difference between these two shaking events is shape of wave: one is positive tapered sinusoidal wave, and the other one is negative tapered sinusoidal wave. The vertical black solid line implied the 13th second of shaking duration of two shaking events in test NCU 2, which points out the trough and the crest of acceleration signal wave in NCU 2-M1 and NCU 2-M2, respectively. It shows that there is a phase difference of 180 degrees. In addition, the spikes

are observed in the direction of positive acceleration both in these two events, which indicates that significant spikes occur when the direction of inertial force is in the direction of the dip of the slope.

18.5.2 Ground Surface Deformation

The horizontal displacement of surface markers was recorded by cameras during centrifuge modeling tests, and the settlement of surface markers was measured after test. Figure 18.22a–c illustrates the movement of surface markers in tests NCU 1, NCU 2, and NCU 3, respectively. The *x*-axis and *y*-axis correspond to the boundary of the rigid container. The dimensions of container are 767 mm in the *x*-axis and 355 mm in the *y*-axis. The positive part of the *x*-axis indicates the uphill side of slope.

All the surface markers moved to downslope after Motion 1 and Motion 2 in each case. The No. A array and No. B array slightly moved to the positive *y*-axis due to the inertial force during centrifuge spinning; contrarily, the No. C array slightly moved to the negative *y*-axis due to the reflection of inertial force to the rigid boundary during centrifuge spinning.

To compare the *x*-component of displacement in cases NCU 1-M1, NCU 2-M1, and NCU 3-M1, the conditions of three motions have the same cycles and frequency, but the different peaks of base acceleration are 0.27 g, 0.22 g, and 0.18 g, respectively. The surface markers have the largest relative displacement at the downhill part in case NCU 3-M1 which is subjected to the lowest PBA. According to the average displacement in the *x*-axis direction of all surface markers in three tests, the displacements of surface markers of No. 3 array and No. 4 array are larger than those of others arrays.

Figure 18.22a shows the comparison of the displacements of surface markers induced by first main-shaking (M1) and second main-shaking (M2) in NCU 1. The difference between M1 and M2 is at the waveform: one is tapered sinusoidal wave (M1), and the other one is sinusoidal wave (M2). The *x*-axis displacement of surface markers induced by NCU 1-M2 is less than that induced by NCU 1-M1, perhaps because the relative density of strata increased after once destructive shaking. The largest displacement is recorded at No. 4 array. Figure 18.22b, c also illustrates displacement of each surface markers induced by first main-shaking (M1) and second main-shaking (M2) in both NCU 2 and NCU 3, correspondingly. The *x*-axis displacement of surface markers induced by NCU 2-M2 is less than that induced by NCU 2-M1, perhaps because the relative density of strata increased after once large shaking. The largest displacement happened at No. 3 array and No. 4 array. By different manner, the *x*-axis displacements of surface markers induced by NCU 3-M1 and NCU 3-M2 are almost the same.

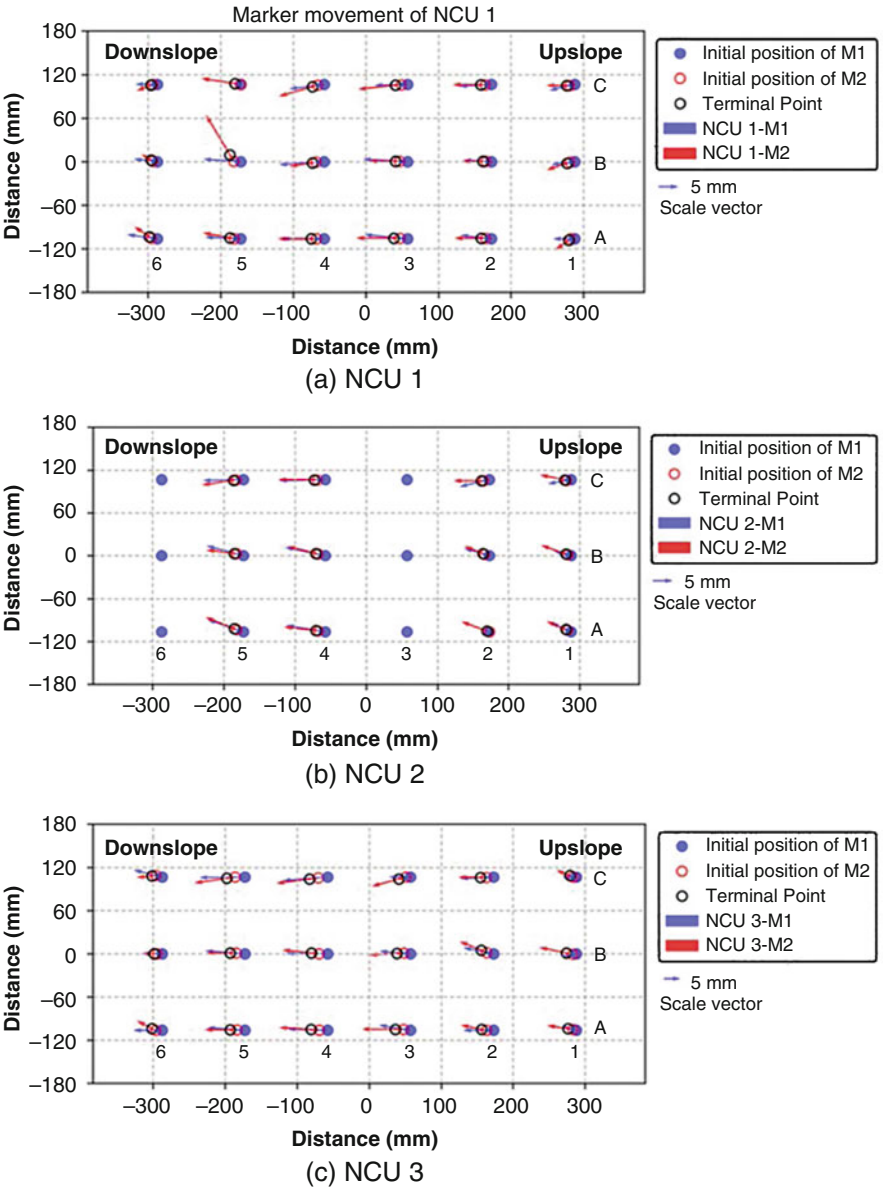

Fig. 18.22 Movement of each surface markers after first main-shaking (M1) and the second main-shaking (M2) in tests of NCU 1 to NCU 3. (**a**) NCU 1, (**b**) NCU 2, and (**c**) NCU 3

18.5.3 Underground Deformation

The spaghetti noodles were inserted into the strata perpendicularly to the horizontal plane of rigid box. After test NCU 2, the profile of strata as in Figs. 18.23 and 18.24 shows the obvious deformation of noodles. The horizontal displacement of noodles in each test is listed in Tables 18.4a, 18.4b, and 18.4c. All of the spaghetti noodles are recorded to move in the downhill direction, and the horizontal displacement decreases along the depth.

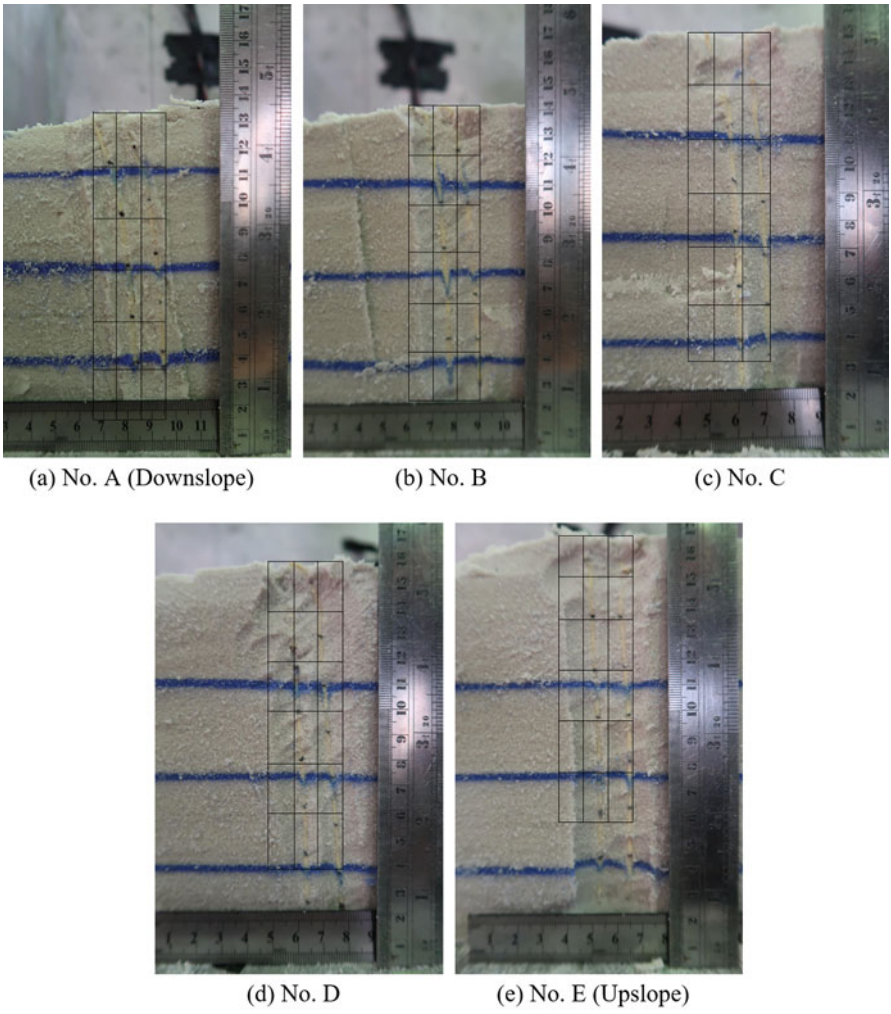

Fig. 18.23 Deformation of spaghetti noodles at different position. (**a**) No. A (Downslope), (**b**) No. B, (**c**) No. C, (**d**) No. D, and (**e**) No. E (Upslope)

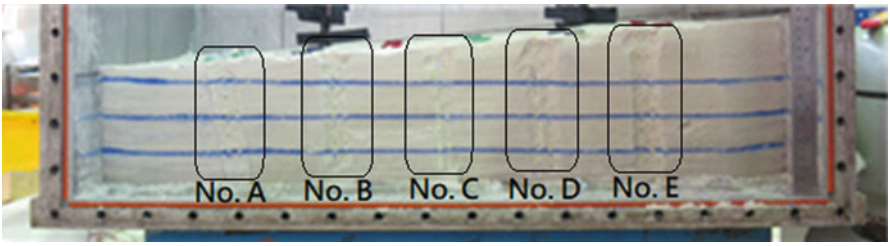

Fig. 18.24 Results of spaghettis in NCU 2

Table 18.4a Horizontal displacement of NCU 1

Depth under the ground surface (m)	No. A	No. B	No. C	No. D	No. E
0	0.40	0.30	0.44	0.43	0.33
−0.5	0.25	0.22	0.34	0.29	0.21
−1.0	0.16	0.16	0.26	0.22	0.13
−1.5	0.09	0.08	0.09	0.16	0.08
−2.0	0.03	0.03	0.10	0.09	0.03
−2.5	0.00	0.00	0.04	0.04	0
−3.0	–	–	0	0	0

Table 18.4b Horizontal displacement of NCU 2

Depth under the ground surface (m)	No. A	No. B	No. C	No. D	No. E
0	0.51	0.35	0.30	0.36	0.21
−0.5	0.26	0.21	0.18	0.18	0.10
−1.0	0.14	0.10	0.12	0.14	0.08
−1.5	0.07	0.08	0.08	0.12	0.04
−2.0	0.04	0.04	0.05	0.07	0
−2.5	0.00	0.03	0.03	0.04	0
−3.0	–	–	0	0	0

Table 18.4c Horizontal displacement of NCU 3

Depth under the ground surface (m)	No. A	No. B	No. C	No. D	No. E
0	0.65	0.62	0.65	–	0.55
−0.5	0.49	0.46	0.39	–	0.31
−1.0	0.23	0.25	0.10	–	0.14
−1.5	0.13	0.07	0.03	–	0.03
−2.0	0.03	0.03	0.03	–	0.01
−2.5	0.00	0.00	0.00	–	0.01
−3.0	–	–	–	–	0.00

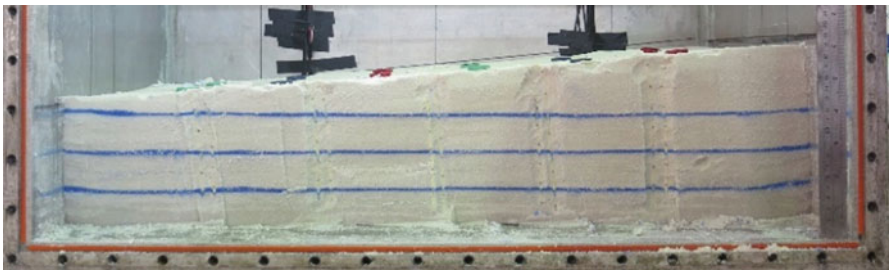

Fig. 18.25 The profile of model after spinning

Table 18.5 The settlement at each sand layer in prototype scale

	NCU 1	NCU 2	NCU 3
Top layer (m)	0.0052	0.0078	0.0052
Mid layer (m)	0	0.0052	0.0052
Bot layer (m)	0	0	0

18.5.4 Blue Thin Sand Layers

The three horizontal blue sand layers were pluviated; during the pluviation process, all of three sand layers are parallel to the plane of the bottom of rigid container. The depths under the ground surface of each color sand layer are 1 m, 2 m, and 3 m, respectively, which correspond to the depth of pore water pressure transducers P4, P3, and P2. The model would be cut after tests; as shown in Fig. 18.25, three color sand layers are still observed to be parallel to the plane of rigid container bottom, but the two upper layers have slight settlement after test, as shown in Table 18.5, and the pore water transducers were still attached within the color sand layers.

18.6 Conclusions

Three centrifuge modeling tests were conducted to simulate a 5-degree-inclined slope of 4-m-deep-saturated sandy ground subjected to different input motions. There are two kinds of main-shaking which includes Motion 1 and Motion 2 in each test. Motion 1 is following the exercise of LEAP-UC-2017, and Motion 2 is designed to observe the effect of different input motions for the responses of soil liquefaction. From the test results, the conclusions are fourfold: (1) the prominent amplitudes of spikes appear in the phase of the positive acceleration during both kinds of waveform which are tapered sinusoidal wave and uniform sinusoidal wave motions, which indicates that the pulses of acceleration are more prominent in the direction of the slope dip; (2) the surface markers move toward the dip direction along the x-axis, and additionally, a component of deformation in the transverse (y-direction) occurs in some events, which might be caused by a small bucket angle

error or perhaps by Coriolis forces; and (3) the magnitude of lateral spreading decreases with depth in the strata, as there is negligible lateral spreading in the bottom meter of the 4 m thick soil deposit. (4) The pore water pressure transducers did not move relative to the colored sand layers after destructive shaking.

Acknowledgments The authors would like to express their gratitude for the financial support from the Ministry of Science and Technology, Taiwan (ROC) (MOST 106-2628-E-008 -004 -MY3) and the technical support from the Experimental Center of Civil Engineering, National Central University. Their support has made this study and future research possible and efficient.

References

Carey, T. J., Stone, N., & Kutter, B. (2019). Grain size analysis and maximum and minimum dry density of Ottawa F-65 sand for LEAP-UCD-2017. In B. Kutter et al. (Eds.), *Model tests and numerical simulations of liquefaction and lateral spreading: LEAP-UCD-2017*. New York: Springer.

Kutter, B., Carey, T., Hashimoto, T., Zeghal, M., Abdoun, T., Kokalli, P., Madabhushi, G., Haigh, S., Hung, W.-Y., Lee, C.-J., Iai, S., Tobita, T., Zhou, Y. G., Chen, Y., & Manzari, M. T. (2017). LEAP-GWU-2015 experiment specifications, results, and comparisons. *International Journal of Soil Dynamics and Earthquake Engineering, 113*, 616–628. https://doi.org/10.1016/j.soildyn.2017.05.018.

Kutter, B. L., Carey, T. J., Stone, N., Bonab, M. H., Manzari, M., Zeghal, M., Escoffier, S., Haigh, S., Madabhushi, G., Hung, W.-Y., Kim, D.-S., Kim, N.-R., Okamura, M., Tobita, T., Ueda, K., & Zhou, Y.-G. (2019). In B. Kutter et al. (Eds.), *Model tests and numerical simulations of liquefaction and lateral spreading: LEAP-UCD-2017*. New York: Springer.

Manzari, M. T., Kutter, B. L., Zeghal, M., Iai, S., Tobita, T., Madabhushi, S. P. G., Haigh, S. K., Mejia, L., Gutierrez, D. A., & Armstrong, R. J. (2015). LEAP projects: Concept and challenges. In *Proceedings: Fourth International Conference on Geotechnical Engineering for Disaster Mitigation and Rehabilitation (4th GEDMAR), 2014 Sept 16–18*. Kyoto: Taylor & Francis.

Okamura, M., & Inoue, T. (2012). Preparation of fully saturated model for liquefaction study. *International Journal of Physical Modeling in Geotechnics, 12*(1), 39–46.

Open Access This chapter is licensed under the terms of the Creative Commons Attribution 4.0 International License (http://creativecommons.org/licenses/by/4.0/), which permits use, sharing, adaptation, distribution and reproduction in any medium or format, as long as you give appropriate credit to the original author(s) and the source, provide a link to the Creative Commons license and indicate if changes were made.

The images or other third party material in this chapter are included in the chapter's Creative Commons license, unless indicated otherwise in a credit line to the material. If material is not included in the chapter's Creative Commons license and your intended use is not permitted by statutory regulation or exceeds the permitted use, you will need to obtain permission directly from the copyright holder.